ACS APPLIED MATERIALS & INTERFACES

Research Article

www.acsami.org

Enhanced Field Emission Properties from CNT Arrays Synthesized on Inconel Superalloy

S. Sridhar,[†,‡] L. Ge,[‡] C. S. Tiwary,[‡,⊗] A. C. Hart,[‡] S. Ozden,[‡] K. Kalaga,[‡] S. Lei,[‡] S. V. Sridhar,[§] R. K. Sinha,[†] H. Harsh,[⊥] K. Kordas,[∥] P. M. Ajayan,[‡] and R. Vajtai*[,‡]

[†]Department of Applied Physics, Delhi Technological University (Formerly Delhi College of Engineering), Bawana Road, Delhi 110042, India

[‡]Department of Material Science and NanoEngineering, Rice University, Houston, Texas 77005, United States

[§]Department of Chemical and Biomolecular Engineering, Rice University, Houston, Texas 77005, United States

[⊥]Department of Physics, Jamia Millia Islamia, New Delhi 110025, India

[∥]Microelectronics and Materials Physics Laboratories, Department of Electrical Engineering, University of Oulu, P.O. Box 4500, FI-90014 Oulu, Finland

[⊗]Materials Engineering, Indian Institute of Science, Bangalore, Karnataka 560012, India

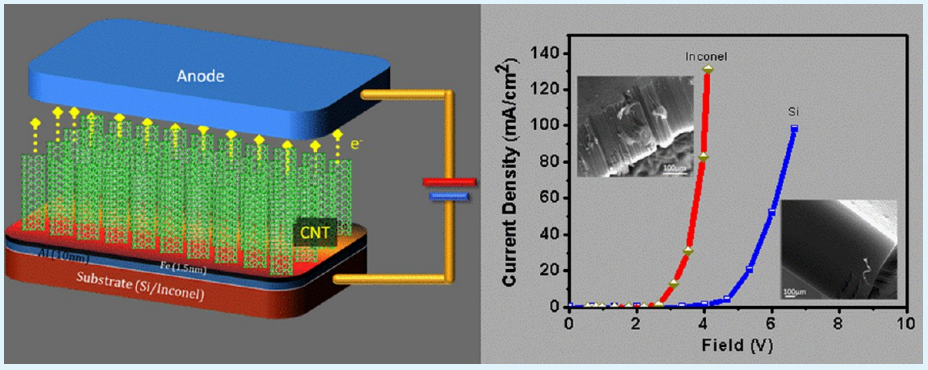

ABSTRACT: One of the most promising materials for fabricating cold cathodes for next generation high-performance flat panel devices is carbon nanotubes (CNTs). For this purpose, CNTs grown on metallic substrates are used to minimize contact resistance. In this report, we compare properties and field emission performance of CNTs grown via water assisted chemical vapor deposition using Inconel vs silicon (Si) substrates. Carbon nanotube forests grown on Inconel substrates are superior to the ones grown on silicon; low turn-on fields (~1.5 V/μm), high current operation (~100 mA/cm^2) and very high local field amplification factors (up to ~7300) were demonstrated, and these parameters are most beneficial for use in vacuum microelectronic applications.

KEYWORDS: *carbon nanotube, water assisted CVD, adhesion, field emission, ohmic contact*

INTRODUCTION

Since the reports made by Heer et al.[1] and Rinzer et al.,[2] on the field emission from films and individual multiwalled carbon nanotubes (MWCNTs), respectively, various experimental studies on the field emission of MWCNTs grown using various techniques on different substrates have been pursued.[3−15] Reliability and reproducibility are the biggest aspects needing improvement when using CNTs in field emission devices; electrical breakdown and current degradation are the two major limiting factors of the reliability of CNT based field emitters. The electrical breakdown is a sudden discharge caused by an avalanche of charged particles above a certain threshold field. The process is associated by the evaporation of electrode materials and/or surface adsorbed impurities as a consequence of electron bombardment of the anode, resistive heating of the sharp cathode or simple desorption of surface impurities so that a low pressure vapor forms in the proximity of the electrodes.[16] Above the threshold field, the vapor undergoes ionization and sparking, similar to that in ordinary low pressure gases, takes place.[17] On the other hand, the emission current degradation is a slow process that occurs below the threshold field. Heating by the emission current and subsequent evaporation of the electrode materials results in a gradual loss, structural collapse and deterioration of the cathode. Apart from thermal and electrical stability of the electrode materials, high quality robust electrical contacts that are interfacing the emitter back side are also vital for multiple reasons. First, the contact must be uniform along the entire interface to allow optimal, uniform

Received: November 8, 2013
Accepted: January 3, 2014
Published: January 13, 2014

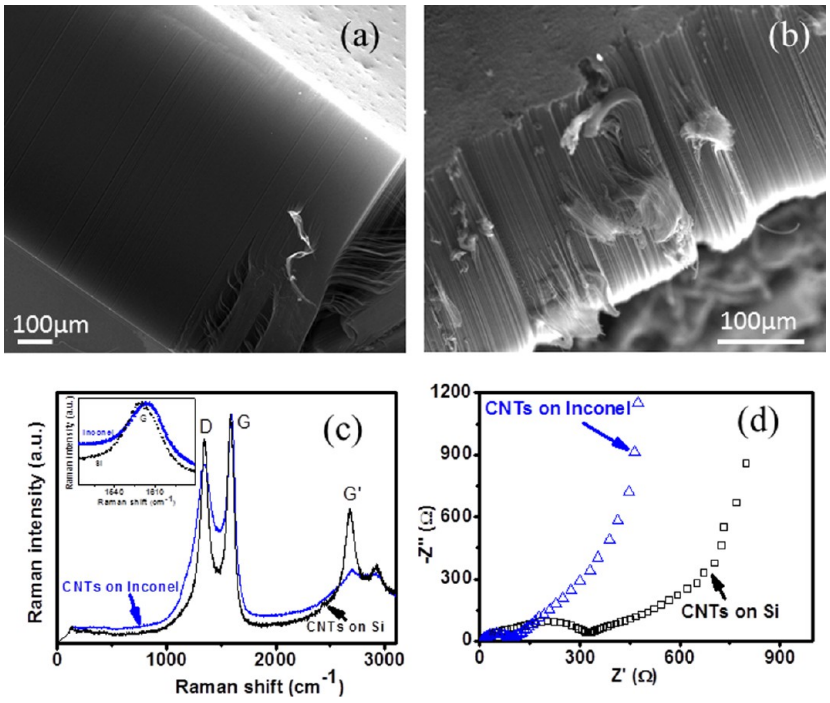

Figure 1. SEM images of CNT films grown on (a) Si and (b) Inconel substrates showing that the CNTs on Si are longer when compared with those on Inconel. (c) Raman spectra of films synthesized on the two substrates (the inset shows the shifted peak position of the G band) and (d) Nyquist plots of the films (on the substrates) measured by electrical impedance spectroscopy using electrochemical lithium half-cell of MWCNTs grown on silicon and Inconel as anodes.

current densities throughout the joint area. This is especially important for carbon nanotube forests, to ensure each nanotube is in direct electrical contact with the substrate with similar contact resistance all around at the interface eliminating the formation of hot spots. Second, good ohmic contacts at the CNT−substrate interface introduce only minor series resistances in the emitter circuit thus resulting in higher emission currents (when voltage regulated) or lower interfacial losses (when current regulated). Third, mechanical strength, or good adhesion, between the nanotube/catalyst and the substrate interface is also an important criterion to minimize problems related to delamination of the emitter material from the back side contact.[18−21]

The above list of requirements suggests two kinds of technical approaches that may offer feasible and reasonably simple solutions to meet the stringent thermal, mechanical and electrical boundary conditions. One solution is a solder transfer of CNT films to electrically conductive surfaces, which has been proven to be a robust and versatile method to obtain joints with excellent structural, thermal and electrical integrity.[22−27] The other, more feasible approach is the direct growth of CNTs on conductive surfaces. As demonstrated previously, growing CNTs on metal substrates or on alloys containing one of the common catalyst metals can result in CNT films of high footprint density, which is electrically advantageous.[28−30] For instance, Talapatra et al.[31] estimated an average total contact resistance of aligned CNTs on Inconel to be about 500 Ω, whereas measurements carried out on similar structures by Halonen et al.[32] showed the contact resistance is as low as ∼10 Ω (for a pattern footprint area of ∼0.4 cm^2). Although relatively low turn-on fields are observed for such devices, the maximum emission current densities reported were typically not higher than 10 mA/cm^2.[32−36] For CNTs to be used in field emission devices, it is not only essential to develop techniques to grow CNTs on conducting substrates but also to get good current density besides reducing the turn on and threshold voltages.

In this paper, we report the growth of CNTs on Inconel and Si substrates in water assisted CVD and compare their field emission behavior. CNTs grown on Inconel exhibited excellent field emission properties: the maximum current densities from the produced emitters were around 100 mA/cm^2. Although CNTs on Si substrates also yielded high initial current densities (>100 mA/cm^2), early arcing and rapid failure of the devices indicate their limited use in high current density applications. The results presented here may be adopted for CNT based cold cathodes suitable for high power microwave vacuum devices and also for long-lifetime low-power applications.

EXPERIMENTAL SECTION

Vertically aligned MWCNTs were synthesized using a water assisted CVD process on Si and Inconel 718 substrates coated previously with 10 nm Al buffer and 1.5 nm Fe catalyst layers using e-beam evaporation (as shown in Figure 1, inset). For CNT growth, the substrate is inserted into a quartz tube inside a furnace and initially purged with argon, then heated up to 775 °C under Ar/H_2 (15% H_2/balance argon). Once the growth temperature, Ar/H_2 is bubbled through water and the carbon source, ethylene, is flown into the reactor. The CNTs are grown for 30 min and, finally, the furnace is cooled under Ar.

Scanning electron microscopy (SEM, FEI Quanta 400 ESEM FEG) and transmission electron microscopy (JEOL 2100 F TEM) were used for sample characterization. Raman spectroscopy was performed using a Renishaw inVia Raman Microscope (laser wavelength of 514 nm). For the field-emission measurements, the silicon (Si) and Inconel substrates with CNTs were used as the cathode and ITO coated glass plate as the anode. The cathode and anode mounting stands are machine ground to ensure that they are perfectly parallel. The whole sample assembly was kept inside a vacuum chamber evacuated to at least 2×10^{-6} Torr, and the distance between the cathode and the

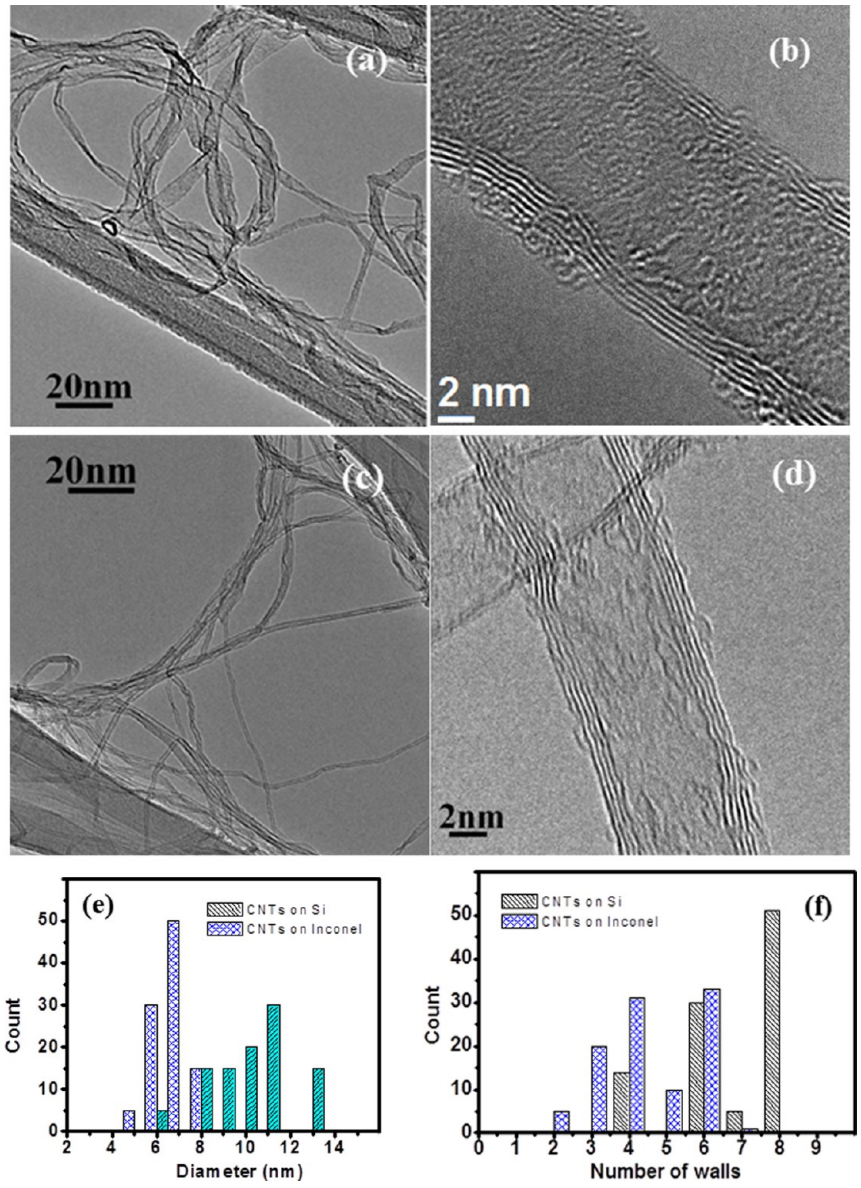

Figure 2. Transmission electron micrographs of CNTs grown (a), (b) on Si and (c), (d) on Inconel substrates. Panels (e) and (f) display the nanotube diameter and wall number distribution plots, respectively.

anode was maintained at 200 μm through a spring loaded micrometer gauge. The CNT sample is mounted on the cathode stand and I–V measurements are done using a Keithley 2410 instrument.

Electrical impedance spectroscopy (EIS) measurements were performed using a two electrode setup with the CNTs on the substrate as the working electrode and lithium metal as the counter/reference electrode. In this, 1 M $LiPF_6$ in 1:1 v/v mixture of ethylene carbonate (EC) and dimethyl carbonate (DMC) is used as the electrolyte and a glass microfiber filter membrane as the separator. The EIS measurements were conducted over 70 kHz to 10 mHz by applying a 10 mV dc bias.

RESULTS AND DISCUSSION

Figure 1a,b displays SEM images of the CNTs grown on Si and Inconel, respectively. The CNTs are vertically aligned via a self-supporting mechanism; according to scanning and transmission electron microscopy analyses, the CNTs grown on Inconel are more tangled and have smaller diameters compared to those grown on Si (Figure 2). Because the same amount of iron is deposited on both substrates, the catalyst interaction with the surface is the only plausible explanation for the differences. One main reason is the different surface roughness of the two substrates. The smooth polished single crystal of Si, in contrast with the rolled foil of the polycrystalline metal alloy of Inconel, ensures that the nanotubes grow parallel with each other. On the other hand, the different chemical qualities and thus surface energy of the two substrates influence the wetting properties of the catalyst metals which affect the catalyst island morphology, size and surface density when heating the samples to the growth temperature resulting in differences in the nanotube diameter distributions for the two substrates. Furthermore, the Inconel substrate itself can also act as an additional catalyst resulting in thinner and denser CNTs. It can be seen that the CNTs on Si are longer when compared with those grown on Inconel most likely due to the partial tangling of the nanotubes and more efficient diffusion of the Al/Fe catalyst into the polycrystalline metal than the single crystal Si surface.

The Raman spectra collected from both samples are plotted together after being normalized to the G band intensity

maximum. Raman analysis in Figure 1c shows the typically observed 3 main distinct bands, the D band (disorder) around 1350 cm^{-1}, the G band (graphitic peak) around 1580 cm^{-1} and the G′ band (long-range order) around 2700 cm^{-1} for the CNTs on both types of substrates. There is a minor shift in the D band and G band positions for the CNTs grown on the two substrates due to their different diameter distribution and the number of walls (Figure 2e,f). The D peak arises due to the formation of sp^3 and dangling sp^2 bonds on the CNT side walls as well as from the deposition of amorphous carbon; the G peak arises from graphitic sp^2 carbon in the nanotubes; the G′ peak is the indicator of long-range order present within the CNTs. For these CNTs, we obtained the intensity ratio I_D/I_G of 0.78 and 0.91 for Inconel and Si, respectively, and the values are very close to the values reported earlier for CNTs synthesized on Inconel.[37]

Electric impedance spectroscopy measurements performed for CNTs grown on both Si and Inconel substrates suggest the structures are sufficiently conductive for emitter applications (Figure 1d). It can be seen from the Nyquist plots that the contact resistance between the CNT and Si is ∼320 Ω/cm^2 whereas for the CNT-Inconel contact it is ∼90 Ω/cm^2. The semicircles in the impedance spectra indicate the presence of a capacitive component most likely caused by the nanotube films of large specific surface area.

From the TEM analysis (Figure 2a–d), it is clear that the number of walls and also the average diameter of CNTs grown on Si are higher than those synthesized on Inconel. TEM analysis also reveals the presence of more amorphous carbon on the surface of the CNTs in the case of Si as compared to those grown on Inconel substrates.

Initially, the CNTs grown on both substrates demonstrated excellent field emission properties. From the J–E curves displayed in Figure 3, we observe that the initial current density of the CNT array grown on Si is higher than that for the corresponding sample obtained on Inconel (131 mA/cm^2 vs 99 mA/cm^2). Initially, the turn-on field (which is the field required to give a current density of 10 μA/cm^2) for the sample grown on Si (2.2 V/μm) is less than that for the nanotubes grown on Inconel (3.4 V/μm). However, the turn-on field for the latter samples decreased considerably from 3.4 to ∼1.5 V/μm after arcing. The threshold field, i.e., the field required to reach a current density of 10 mA/cm^2, also shows a similar tendency. For the CNT films grown on Si, it gradually increases; meanwhile a significant decrease of the corresponding threshold value is observed for the samples synthesized on the metal alloy substrate (from ∼5.0 to 2.8 V/μm). The increase in the turn on and threshold fields as well as the early device failure for the films grown on Si might be because of the structural damage of the emitters[38] as also indicated by the voids and fused CNTs visible in SEM images (Figure 4).

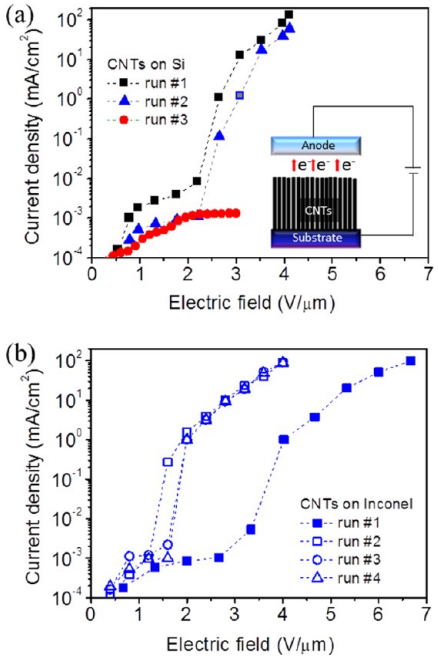

Figure 3. Plots of emission current density as a function of applied electric field in repeated experiments for CNTs grown on (a) Si and (b) Inconel.

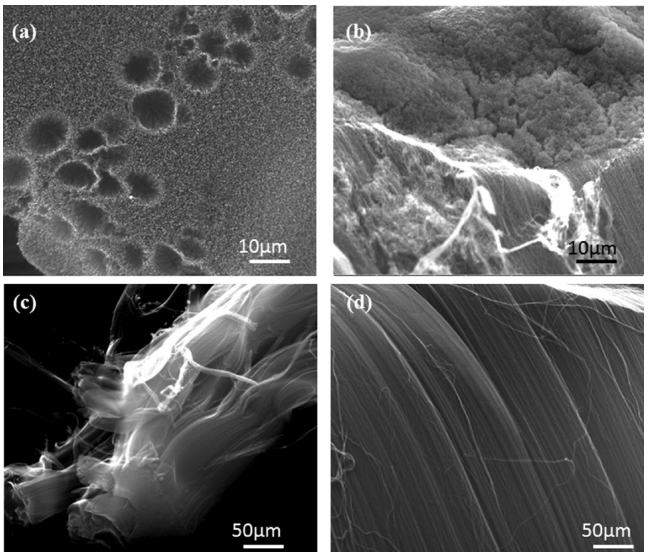

Figure 4. SEM images of the samples after field emission. CNT films (a) on Si, top view, (b) on Inconel, top view, (c) on Si side view and (d) on Inconel, top view. Microscopic voids in the used films on Si show the structural instability in contrast with the continuous surface of the films grown on Inconel.

The causes of CNT degradation on the Si substrate can be associated with a number of different mechanisms: (1) Poor adhesion of CNTs to the substrate and consequent peeling, (2) high and/or inhomogeneous contact resistance between the CNTs and the substrate resulting in large local current densities and excessive joule heating and (3) at high electric fields, resistive heating and related stress due to thermal expansion coefficient mismatch at the CNT–substrate junction causing mechanical failure. According to Okai et al.,[18] the strong repulsive electrostatic forces may also be a reason for the electrical breakdown during field emission. As reported in our earlier work,[39,40] when the electric field between the anode and the cathode is increased, the dipole resulting from the concentration of electrons in the tips of carbon nanotubes will enhance the static electric force and pull the carbon nanotubes off from the substrate, leading to an abrupt drop of emission current. As noticed by Wang et al.,[38] the electrostatic force created by the flow of emission current acting in the tip of nanotube can induce a split or even burning of the emitters. On the other hand, there was no obvious electrical breakdown in

the case of the sample grown on Inconel while the emission threshold fields were improving with use. The superior field emission properties and reliability of the nanotube films grown on Inconel as compared to those on Si are inevitable and can be explained by the good electrical and thermal interface between the nanotubes and the metallic substrate. The excellent electrical contact ensures uniform current distribution in the entire cross-section of the emitter, thus eliminating the formation of hot spots and also avoiding the evolution of excess Joule heat in local microscopic volumes at the nanotube−substrate interface as well as at the tips of the nanotubes. The improved overall field emission performance of the Inconel-supported films may be due to localized cleaning caused by mild arcing at the tips of the nanotubes. In addition, a uniform fusing of the CNT−catalyst−Inconel interface caused by the current might have also taken place by which the electrical and mechanical properties of the interfacial contact are improved.

Another important aspect is the field enhancement factor (β) that describes how much the emitter tips amplify the macroscopic electric field around the sharp and highly curved apexes. As predicted by Mc. Clain et al.,[41] as the diameter of the CNTs decreases (in our case, the CNTs grown on Inconel), the emission field decreases with a corresponding increase in field amplification. The total emission current depends on the field enhancement factor and, accordingly, on the diameter of the CNTs, the smaller the diameter the higher the emission current. From the slope of the linearized Fowler−Nordheim plot (i.e., by plotting $\ln(J/U^2)$ versus $1/U$ (Figure 5), where J is the current density and U is the voltage drop on the emitter, β can be determined. The slope is $m = (Bd\phi^{3/2})/\beta$, where B is a constant with the value of 6.83×10^9 V eV$^{-3/2}$ m^{-1}, ϕ is the work function of the emitter material (~5 eV for CNTs) and d is the distance between the cathode and the anode (200 μm in our case).

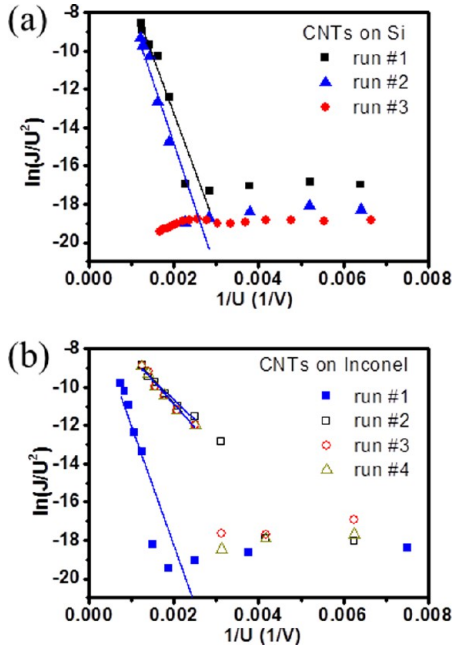

Figure 5. Fowler−Nordheim curves of the samples grown on (a) Si and (b) Inconel substrate (from the data in Figure 3). The corresponding field enhancement factors are determined from the linear fitting slopes in the high field regime.

The enhancement factors for both types of emitter structures are very similar having values of ~2500. In the case of the Si-supported CNT films, this value remained unchanged as long as the emitters were functional. Interestingly, for the nanotube films synthesized on Inconel, this initial field amplification value is abruptly increased to ~7300 when repeating the measurement on the same device and then it kept the increased value in the subsequent tests. Such a substantial increase in the field amplification is a consequence of surface cleaning by the mild arcing in the course of the first emission experiment but also sharpening of the nanotube tips might have taken place as suggested by Talapatra and co-workers.[31] Although the initial values for β are rather close to the ones reported for nanotube films in the literature (i.e., typically between 500 and 3000),[1,5,31,42,43] the improved enhancement factors are considerably higher than those.

CONCLUSIONS

In conclusion, vertically aligned CNTs on Inconel substrates grown via water assisted chemical vapor deposition have shown excellent field emission properties clearly outperforming similar films synthesized on Si substrates. The field emitter devices synthesized on the metallic substrate have low turn-on fields (~1.5 V/μm), enable high current operation (~100 mA/cm^2) and show very high local field amplification with factors up to ~7300. These properties, along with their increased reliability, make the demonstrated structures as a potential candidate for future flat panel displays based on CNT-electron emitters.

AUTHOR INFORMATION

Corresponding Author

*R. Vajtai. E-mail: Robert.Vajtai@rice.edu.

Notes

The authors declare no competing financial interest.

ACKNOWLEDGMENTS

C. S. Tiwary thanks IISc (Indian Institute of Science), Bangalore for their support. A. Hart, R. Vajtai and P.M. Ajayan acknowledge financial support from U.S. Army Research Laboratory/Army Research Office (No. W911NF).

REFERENCES

(1) Heer, W. A.; Chatelain, A.; Ugarte, D. *Science* **1995**, *270*, 1179−1180.
(2) Rinzler, A. G.; Hafner, J. H.; Nikolaev, P.; Lou, L.; Kim, S. G.; Tomanek, D. *Science* **1995**, *269*, 1550−1553.
(3) Saito, Y.; Hamaguchi, K.; Hata, K.; Uchida, K.; Tasaka, Y.; Ikazaki, F.; Yumura, M.; Kasuya, A.; Nishina, Y. *Nature* **1997**, *389*, 554−555.
(4) Wang, Q. H.; Corrigan, T. D.; Dai, J. Y.; Chang, R. P. H.; Krauss, A. R. *Appl. Phys. Lett.* **1997**, *70*, 3308−3310.
(5) Bonard, J. M.; Maier, F.; Stockli, T.; Chatelain, A.; Heer, W. A.; Salvetat, J. P.; Forro, L. *Ultramicroscopy* **1998**, *73*, 7−15.
(6) Teo, K. B. K.; Chhowalla, M.; Amaratunga, G. A. J.; Milne, W. I.; Pirio, G.; Legagneux, P.; Wyczisk, F.; Pribat, D.; Hasko, D. G. *Appl. Phys. Lett.* **2002**, *80*, 2011−2013.
(7) Chen, Y.; Sun, Z.; Chen, J.; Xu, N. S.; Tay, B. K. *Diamond Relat. Mater.* **2006**, *15*, 1462−1466.
(8) Siegal, M. P.; Miller, P. A.; Provencio, P. P.; Tallant, D. R. *Diamond Relat. Mater.* **2007**, *16*, 1793−1798.
(9) Pandey, A.; Prasad, A.; Moscatello, J. P.; Engelhard, M.; Wang, C.; Yap, Y. K. *ACS Nano* **2013**, *7*, 117−125.
(10) Su, J.; Guo, D. Z.; Xing, Y. J.; Zhang, G. M. *Phys. Status Solidi A* **2013**, *210*, 349−355.

(11) Ren, H.; Yang, L.; Zhang, Y. *J. Phys.: Conf. Ser.* **2013**, *418*, 012007.
(12) Bhattacharya, S.; De, D.; Ghosh, S.; Ghatak, K. P. *J. Comput. Theor. Nanosci.* **2013**, *10*, 1−5.
(13) Atthipalli, G.; Epur, R.; Kumta, P. N.; Gray, J. L. *J. Vac. Sci. Technol., B: Nanotechnol. Microelectron.: Mater., Process., Meas., Phenom.* **2011**, *29*, 04D102.
(14) Sun, P. C.; Deng, J. H.; Cheng, G. A; Zheng, R. T.; Ping, Z. X. *J. Nanosci. Nanotech.* **2012**, *12*, 6510−6515.
(15) Berhanu, S.; Gröning, O.; Chen, Z.; Merikhi, J.; Kaiser, M.; Rupesinghe, N. L.; Bachmann, P. K. *Phys. Status Solidi A* **2012**, *209*, 2114−2125.
(16) Wijker, W. J. *Appl. Sci. Res., Sect. B* **1961**, *9*, 1−20.
(17) Almy, J. E. *Phys. Rev. (Series I)* **1907**, *24*, 50−59.
(18) Okai, M.; Fujieda, T.; Hidaka, K.; Muneyoshi, T.; Yaguchi, T. *Jpn. J. Appl. Phys.* **2005**, *44*, 2051−2055.
(19) Bonard, J. M.; Klinke, C. *Phys. Rev. B* **2003**, *67*, 115406−115415.
(20) Nessim, G.; Seita, M.; O'Brien, K.; Hart, A.; Bonaparte, R.; Mitchell, R.; Thompson, C. *Nano Lett.* **2009**, *9*, 3398−3405.
(21) Kim, B.; Chung, H.; Chu, K.; Yoon, H.; Lee, C.; Kim, W. *Synth. Met.* **2010**, *160*, 584−587.
(22) Fu, Y.; Nabiollahi, N.; Wang, T.; Wang, S.; Hu, Z.; Carlberg, B.; Zhang, Y.; Wang, X.; Liu, J. *Nanotechnology* **2012**, *23*, 045304.
(23) Kordás, K.; Tóth, G.; Moilanen, P.; Kumpumäki, M.; Vähäkangas, J.; Uusimäki, A.; Vajtai, R.; Ajayan, P. M. *Appl. Phys. Lett.* **2007**, *90*, 1231051−3.
(24) Fu, Y. F.; Qin, Y. H.; Wang, T.; Chen, S.; Liu, J. H. *Adv. Mater.* **2010**, *22*, 5039−5042.
(25) Kumar, A.; Pushparaj, V. L.; Kar, S.; Nalamasu, O.; Ajayan, P. M.; Baskaran, R. *Appl. Phys. Lett.* **2006**, *89*, 163120 1−3.
(26) Tóth, G.; Mäklin, J.; Halonen, N.; Palosaari, J.; Juuti, J.; Jantunen, H.; Kordás, K.; Sawyer, W. G.; Vajtai, R.; Ajayan, P. M. *Adv. Mater.* **2009**, *2*, 211−215.
(27) Mittal, J.; Lin, K. L. *J. Nanosci. Nanotech.* **2013**, *13*, 5590−5596.
(28) Masarapu, C.; Wei, B. *Langmuir* **2007**, *23*, 9046−9049.
(29) Baddour, C.; Fadlallah, F.; Nasuhoglu, D.; Mitra, R.; Vandsburger, L.; Meunier, J. *Carbon* **2008**, *47*, 313−318.
(30) Benito, S.; Lefferts, L. *Carbon* **2010**, *48*, 2862−2872.
(31) Talapatra, S.; Kar, S.; Pal, S.; Vajtai, R.; Ci, L.; Victor, P.; Shaijumon, M.; Kaur, S.; Nalamasu, O.; Ajayan, P. M. *Nat. Nanotechnol.* **2006**, *1*, 112−116.
(32) Halonen, N.; Mäklin, J.; Rautio, A. R.; Kukkola, J.; Uusimäki, A.; Toth, G.; Reddy, L. M.; Vajtai, R.; Ajayan, P. M.; Kordas, K. *Chem. Phys. Lett.* **2013**, *583*, 87−91.
(33) Sung, W.; Kim, W.; Lee, H.; Kim, Y. *Vacuum* **2008**, *82*, 551−555.
(34) Lahiri, I.; Seelaboyina, R.; Hwang, J.; Banerjee, R.; Choi, W. *Carbon* **2001**, *48*, 1531−1538.
(35) Mahanandia, P.; Arya, V.; Bhotla, P.; Subramanyam, S.; Schneider, J.; Nanda, K. *Appl. Phys. Lett.* **2009**, *95*, 083108.
(36) Yi, W.; Yang, Q. *Diam. Relat. Mater.* **2010**, *19*, 870−874.
(37) Atthipalli, G.; Wang, H.; Gray, J. L. *Appl. Surf. Sci.* **2013**, *273*, 515−519.
(38) Wang, Z. L.; Gao, R. P.; Heer, W. A.; Poncharal, P. *Appl. Phys. Lett.* **2002**, *80*, 856−858.
(39) Verma, P.; Gautham, S.; Kumar, P.; Chaturvedi, P.; Rawat, J. S.; Pal, S.; Chaubey, R.; Harsh, H. P.; Vyas, P. K.; Bhatnagar. *J. Vac. Sci. Technol., B: Microelectron. Nanometer Struct.–Process., Meas., Phenom.* **2007**, *25*, 1584−1587.
(40) Srividya, S.; Gautam, S.; Jha, P.; Kumar, P.; Kumar, A.; Ojha, U. S.; Rawat, J. S. B. S.; Pal, S.; Chaudhary, P. K.; Harsh, R.; Sinha, K. *Appl. Surf. Sci.* **2010**, *256*, 3563−3566.
(41) McClain, D.; Wu, J.; Taven, N.; Jiao, J.; McCarter, C.; Richards, C.; Richards, R.; Bahr, D. *J. Phys. Chem. C* **2007**, *111* (20), 7514−7520.
(42) Guillorn, M. A.; Melechko, A. V.; Merkulov, V. I.; Hensley, D. K.; Simpson, M. L.; Lowndes, D. H. *Appl. Phys. Lett.* **2002**, *81*, 3660−3662.
(43) Saito, Y.; Uemura, S. *Carbon* **2000**, *38*, 169−182.